Proceedings of the ASME 2024 43rd International Conference on Ocean, Offshore and Arctic Engineering
OMAE2024
June 9-14, 2024, Singapore, Singapore

OMAE2024-124558

RELATIVE MOTION PREDICTION FOR INTEGRATED FLOATING OFFSHORE WIND TURBINE INSTALLATION SCHEME BASED ON DATA-DRIVEN

Can Ma[1], Taiyu Zhang[1], Zongyuan Yang[1], Yang An[1], Xiang Yuan Zheng[1], Zhengru Ren[1,*]

[1]Institute for Ocean Engineering, Tsinghua University, Shenzhen, China

ABSTRACT

With the development of offshore wind power toward deeper seas, innovative installation methods for floating offshore wind turbines (FOWTs) are urgently needed. A novel installation approach involves a specially designed catamaran that carries multiple preassemblies (tower, hub, and blades are mated onshore) to the installation site. The approach separates the construction of foundations and preassembled upper structures. Carrying multiple preassemblies onboard shortens the transportation time, and only one lifting operation shortens the offshore mating time. Due to the complexity of the offshore environment, irregular relative motions occur between the preassemblies and the floating foundation. Larger relative distances between the mating points (lifted preassembly bottom center point and floating foundation top center point) would increase the outcrossing rate during the mating operation. Artificial neural networks are applied to predict the maximum and minimum relative motions between the two mating points during the implementation of mating operations. The installation scheme is simulated in various sea states using Sima, generating datasets for analysis. Statistical motion data (mean value and low-order central moments) for the past period are used as inputs to the neural network to obtain the maximum and minimum relative motion for the coming period. Simulation results show that the prediction model constructed by the back propagation neural network can predict maximum and minimum values of relative motions with acceptable accuracy. The proposed algorithm enables the prediction of potential hazards during the mating operation of the conceptual installation method, facilitating informed decision-making by the crews.

Keywords: floating offshore wind turbine, artificial neural network, relative motion

1. INTRODUTION

As offshore wind farms develop toward deeper seas, floating offshore wind turbine (FOWT) structures have emerged as an inevitable trend. Marine operation of the floating wind turbines installation also has a series of challenges, such as reducing costs and ensuring safety. Self-elevating vessels are typically equipped with three or four legs, which can be inserted into the seabed. After the legs are positioned, the hull can be lifted away from the wave zone. The length of tension legs [1] limits the application of the self-elevating vessels for the deep-water installation of FOWTs. Wet towing is one of the most commonly used methods for transporting FOWTs. However, wet towing has some disadvantages, such as its slow transport speed and low efficiency, which limits its ability to adapt to long-distance transportation. Hywind Scotland is a practical engineering project applying a large semi-submersible vessel to lift a preassembly and transport it to the installation site. Using the large crane to finish the mating operation between the moored Spar foundation and the preassembly. However, the engagement of the large crane significantly increases the installation cost.

A conceptual tower-nacelle-rotor preassembly lifting method proposed by the SFI MOVE [2, 3] uses the low-high lifting gripper to lift the preassembly, avoiding the use of large cranes. A catamaran is used as the installation vessel to carry multiple preassemblies to the installation site. The installation vessel is equipped with sliding grippers to maintain the relative motions in the horizontal plane between the installation and the moored Spar foundation. A passive roller at the end tip of each sliding gripper so that the Spar foundation can move in the z-direction. A dynamic positioning system (DP) is also equipped to offset the drifting motion of the vessel. The method is an innovative approach to avoid extremely weather-sensitive high lift operations. It can widen the weather window for installation and reduce the time consumed in transportation. However, it is at the conceptual design stage and needs to be refined in all aspects. Jiang [3] summarises three existing challenges in the tower-nacelle-rotor preassembly lifting method, i.e., structural dynamics, hydrodynamics properties of the two floating structures, and automatic control demands for different stages. To further reduce the motion responses, the small water-plane area twin hull vessel (SWATH)

*Corresponding author: zhengru.ren@sz.tsinghua.edu.cn

[4] can be used as an installation vessel to avoid resonance. Novel gripper designs [5] are also proposed to reduce the effects of external loads. Heave compensation [6], dynamic position system, and fender [7] can improve the system performance. The structural flexibility [8] of the crane is also considered in the dynamic responses of the installation system.

Relative motions between the lifted preassembly and floating foundations during installation influence the success of the mating operation. Many practical issues, especially the relative motions between the mating points (lifted preassembly bottom center point and Spar top center point), need further study. Relative position and velocity of the mating points determine the probability of outcrossing. The outcrossing is defined as relative motions between two mating points that exceed a set safe operating boundary. While the relative motions between mating points can be offset by an active heave compensation system and simulated using software such as Sima or other existing codes, substantial personal and property losses may occur in the event of an accident. So it is essential to predict the relative motions and make early warning based on the predicted results.

Based on the motion prediction research, it can be the basement of control design and decision-making for marine operations (i.e., float-over installation, heavy lifting, aircraft landing, and anti-roll). Most existing research can be divided into such as physical prediction method [9–11] based on the combination of the waves and vessel's hydrodynamic characterisation, autocorrelation function method [12], classic time series prediction method [13], and intelligent prediction method. The autocorrelation function method is based on the vessel's historical motions to predict future motions. Instantaneous autocorrelation function method [14] using the short-time data measurements is further developed to overcome the shortcoming of the short prediction ability. Floating structures' motions usually express non-Gaussian features by suffering the non-Gaussian external loads (i.e., wind and wave). Traditional motion prediction methods based on the linear theory have limited predictive effects. Statistically based extreme value theory also seems to solve the above prediction problem. However, it is difficult to migrate to the implementation of offshore wind turbine installations. The intelligent prediction method does not rely on experts in one field so much and can be based directly on the data itself to realize motion prediction. Artificial neural network (ANN) [15–18] algorithm is one of the intelligent prediction methods, and it has been proved to be an efficient technique in solving nonlinear motion prediction problem. It can rely on simulation-based offline training to obtain the feedforward knowledge, which makes the trained neural networks be used in the installation operation. The progress in sensor technology has facilitated the monitoring of vessel motions, thus contributing to the application of ANN in relative motion prediction.

The significant contributions of this paper are predicting the maximum and minimum values of relative motion between the mating points to decrease the pitfalls of inaccurate weather forecasts. The specific details of motions are unimportant compared to the maximum and minimum values in the mating operation. The paper is organized as follows. In Section 2, the installation system and the methodology are introduced. Section 3 explains the simulation model setup and the workflow of the neural network. Section 4 shows the simulation results of the relative motion of the mating points under different sea states, and the prediction effect based on the neural network is demonstrated. The conclusions of the paper are summarized in Section 5.

2. METHODOLOGY

2.1 System description

This research focuses on a scenario (see Fig.1) in which the foundation has been moored in the installation site, and some lower grippers are used to maintain the relative motions between the installation vessel and the foundation in the horizontal plane. One of the preassemblies onboard is gripped and moved to the stern of the installation vessel, waiting for release. No lowering or lifting operations are performed on the preassembly at the stern. The installation procedure of the proposed installation concept has been described specifically in previous studies [3, 7]. Motion monitoring sensors are installed on the installation vessel and Spar foundation to monitor the motion states. Instead of the installation process details, short-term predictions of the mating points' relative motions are the main challenge studied in this paper.

2.2 Description of relative motion

Global reference frame system $\{n\}$ are defined. The right-hand body-fixed reference frame systems $\{b\}$ of the vessel and the floating foundation are denoted by $\{b_1\}$ and $\{b_2\}$, respectively. The specific orientation of the coordinate axes is shown in Fig.1. Origins of the body-fixed reference frame systems are set at the sea surface.

The vessel and foundation are regarded as rigid bodies, and the lifted preassembly and the preassemblies onboard are considered to be rigidly connected to the vessel. The motion of the mating points can be got in the following relationship

$$p^n_{m,b} = p^n_b + R^n_b l^b_m, \tag{1a}$$

$$\dot{p}^n_{m,b} = \dot{p}^n_b + R^n_b S(\omega) l^b_m, \tag{1b}$$

where p^n_b and $p^n_{m,b}$ represent the positions of the origin of $\{b\}$ and the mating point in $\{n\}$, respectively. l^b_m represent the relative distance between the mating point to the origin of $\{b\}$, R^n_b is the rotation matrix, $S(\cdot)$ represents the vector cross-product calculation (i.e., $\omega \times l^b_m = S(\omega) l^b_m$). Relative motions includes relative displacement and relative velocity. The relative displacement between the mating points δd_p can be expressed as

$$\delta d_p = \| p^n_{m_1,b_1} - p^n_{m_2,b_2} \|^2, \tag{2}$$

where $p^n_{m_1,b_1}$ refers to the position of the lifted preassembly bottom center point in $\{n\}$, $p^n_{m_2,b_2}$ refers to the position of the Spar top center point in $\{n\}$. Moreover, $\delta \dot{d}_p$ represent relative velocity and is the derivative of δd_p. Relative motions between mating points can be further divided into relative motions in the horizontal plane and the vertical plane, shown in Fig.2. The x-z plane is chosen as the plane to focus on the pitch motion of the structures. Motions in different planes can reach maxima and minima magnitudes at different moments. It is necessary to discuss the motion performance of the mating points in different planes.

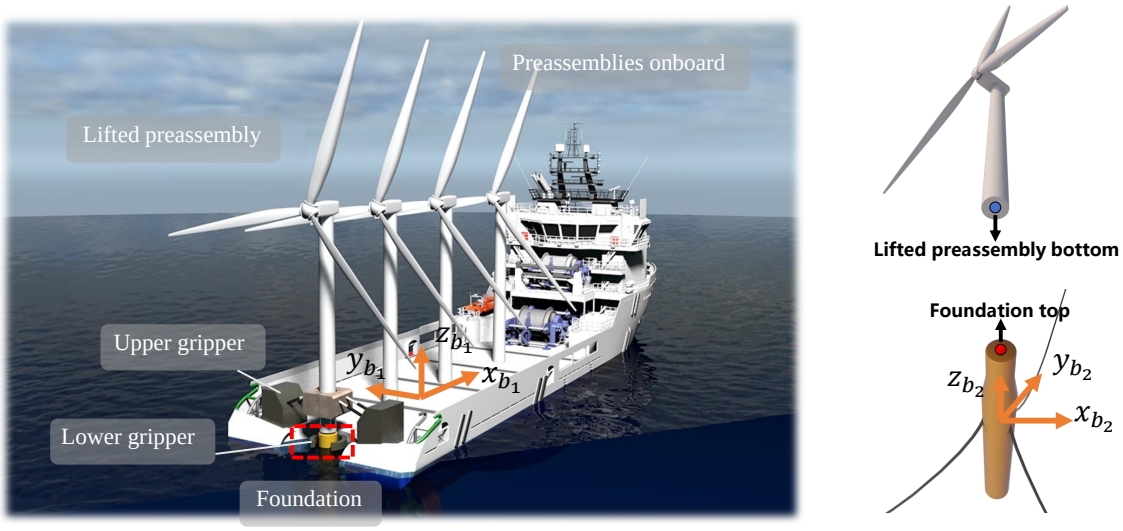

FIGURE 1: Overview of the research scenario and the mating points.

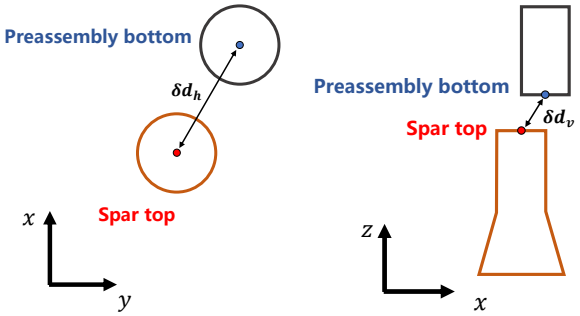

(a) Horizontal plane. (b) Vertical plane.

FIGURE 2: Relative motions between mating points in different planes.

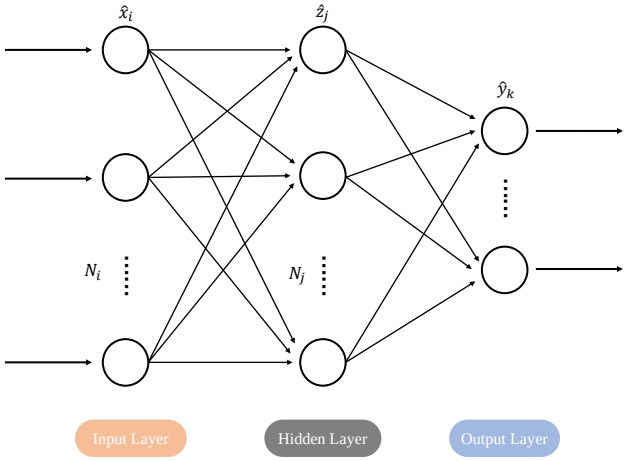

FIGURE 3: Structure of the ANN with one hidden layer.

2.3 Describe of central moment

The prediction of the floating structure's motions in the marine environment is generally based on a statistical concept of a stationary process in most studies. The assumption is made without the necessity to state it. The central moment is a statistical concept that can be used to obtain features of a set of data. Mean value and the k-th orders central moments are given by

$$\mu = E(X), \tag{3a}$$

$$M_k = E(X-\mu)^k, \tag{3b}$$

where X denotes a variable, k denotes the order, μ and M_k denote the mean value and the k-th orders central moments, respectively. In the present paper $k \in \{1, 2, 3, 4\}$. It should be noted that the M_1 is 0. Besides, M_3 and M_4 are skewness and kurtosis, respectively. The skewness explains the amount and direction of the skew. The kurtosis is used to describe the central peak. A higher value of the kurtosis indicates a higher and sharper peak.

2.4 Artificial neural network

An artificial neural network consists of a number of interconnected neurons, and it is divided into the input layer, hidden layer, and output layer. Fig.3 shows the structure of the back propagation (BP) neural network with only one hidden layer. The mathematical relationship among the input neuron, hidden neuron, and output neuron values can be written as

$$\hat{z}_j = g_1\left(\sum_{i=1}^{N_i} \omega_{ij}\hat{x}_i + b_j\right), \tag{4a}$$

$$\hat{y}_k = g_2\left(\sum_{j=1}^{N_j} \omega_{jk}\hat{z}_j + b_k\right), \tag{4b}$$

where $\hat{x}_i$, $\hat{z}_j$, and $\hat{y}_k$ are the values of input neuron, hidden neuron, and output neuron, respectively. ω_{ij} and ω_{jk} are the weighting coefficients. N_i and N_j are the number of neurons in the input layer and hidden layer. $g_1(\cdot)$ and $g_2(\cdot)$ are the activation functions. The neurons of the previous layer are fed through weighting coefficients to the connected neurons of the next layer, and the activation functions with bias in the neurons of the current layer

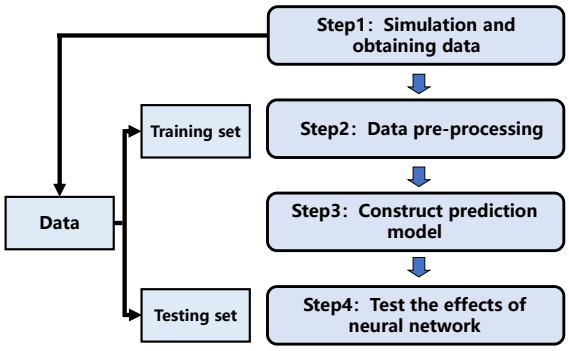

FIGURE 4: Work flow of the simulation.

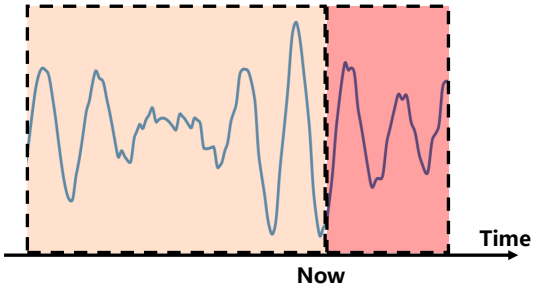

FIGURE 5: Split the time series data.

are transformed to compute the output. The activation function adds a nonlinear representation to the neurons, allowing the neural network to represent complex nonlinear relationships between input and output variables.

The above process is called forward propagation. However, an error e between the predicted output value and the actual output value through the neural network can be expressed as

$$e = \frac{1}{N_k}\sum_{i=1}^{N_k}(y_k - \hat{y}_k)^2, \tag{5}$$

where N_k denotes the number of the output value, y_i denote the actual output value. Finally, back propagation is used to calculate the optimal weighting coefficients.

3. OVERVIEW OF THE SIMULATION AND PREDICTION

3.1 Prediction model construction and validation

The artificial neural networks use amounts of training data to set up a relationship between multiple input and output variables. Data is the basement of training neural network. Advances in sensors have made it possible to monitor the motions of floating offshore structures [19]. Due to the high thresholds of the acquisition of actual motion data, high-fidelity simulations are great substitutes. The specific workflow is shown in Fig.4. Firstly, the installation system is modeled in a Sima, and the motions of the mating points under different sea states are obtained. A split process is performed for the obtained time-range signals for motion. The first 70% of the motion is used as historical data, and the rest is set as future data, shown in Fig.5. For the data used to construct the prediction model, the input variables are the mean value and the central moments ($2nd$ to $4th$ orders) of the relative motions and the relative velocities in the historical data, while the output variables are the maximum and minimum relative displacement and relative velocity of the future data. Normalization is performed for the input variables to

$$\hat{x}_i^* = \frac{\hat{x}_i - \hat{x}_{\min}}{\hat{x}_{\max} - \hat{x}_{\min}}, \tag{6}$$

where $\hat{x}_i^*$ denotes normalized input variables, $\hat{x}_{\max}$ and $\hat{x}_{\min}$ denote the maximum and minimum input variables, respectively. In this paper, only the three-dimensional relative motion prediction is presented, for the motion prediction in the different planes can use the same method. They are not separately listed here to discuss. To verify the prediction accuracy of the neural networks, the predicted results are compared to the original output value in the testing set. The data that make up the testing set can be sensors obtained. The simulation results are used to be the testing set in the paper.

Mean square error (MSE) and coefficient of determination (R^2) are used as the criterion to analyze the prediction accuracy. The expressions of MSE and R^2 are shown as follows

$$\mathrm{MSE} = \frac{\sum_{i=1}^{n}(\hat{y}_i - y_i)^2}{n}, \tag{7a}$$

$$R^2 = 1 - \frac{\sum_{i=1}^{n}(\hat{y}_i - y_i)^2}{\sum_{i=1}^{n}(\bar{y}_i - y_i)^2}, \tag{7b}$$

where $\bar{y}_i$ is the mean of the actual value. MSE reflect the error level between the actual value y_i and the predicted value $\hat{y}_i$. When MSE tends to 0, it indicates a better prediction effect. R^2 ranges from 0 to 1, representing the degree of correlation about the prediction effect.

3.2 Setup of the simulation system

The properties of the catamaran and the Spar foundation are summarized in Table 1. The two structures are modeled as rigid bodies with mechanical and hydrodynamic couplings. The lifted preassembly and the rest preassemblies onboard are considered to be rigidly connected to the vessel. So the motions of the lifted preassembly bottom point can be calculated between the relationship of the vessel motion and the local position of the lifted preassembly bottom point. The local position of the lifted preassembly is related to the lifting height. The initial positioning of the lifted preassembly bottom center point is set to be 2 m above the top of the Spar top center point. Besides, the Spar foundation is moored at the sea bed. The DP system is equipped on the vessel to offset second-order wave, current, and wind loads. Specific parameter settings can be found in Jiang's [3] work.

Long-crested wave loads are generated from Jonswap wave spectrum. The sea states of the simulations are listed in Table 2. Significant wave height H_s, peak period T_p, wave direction, and wave seed are taken into account to evaluate the effect on the relative displacement and relative velocity extremes. Totally $5\times12\times3\times7$=1260 cases are simulated and considered to be the total data set. The simulation duration for each case is set to 1800 s. The time integration step is set to 0.01 s, and the data storage step is set to 0.1 s.

TABLE 1: Properties of the foundation and vessel with preassemblies

Parameter	unit	Catamaran with preassemblies	Foundation
Origin of body reference frame system in $\{n\}$	m	(64,0,0)	(0,0,0)
Center of Gravity (COG) in $\{b\}$	m	(-7.3,0,20.6)	(0,0,-40)
Mass matrix	–	diag(1.8e7,1.8e7,1.8e7, 2.3e10,4.1e10,2.5e10)	diag(1.1e7,1.1e7,1.1e7, 2.8e10,2.8e10,3.7e8)
Mating points in $\{b\}$	m	(-64,0,22)	(0,0,20)

TABLE 2: Sea states

Input parameters	**Values**
Significant wave height H_s (m)	1.0, 1.3, 1.6, 1.9, 2.2
Peak period T_p (s)	6.0, 6.5, 7.0, 7.5, 8.0, 8.5, 9.0, 10.0, 10.5, 11.0, 11.5, 12
Wave seed	1, 2, 3
Wave direction (deg)	0, 30, 60, 90, 120, 150, 180
Simulation time (s)	1800

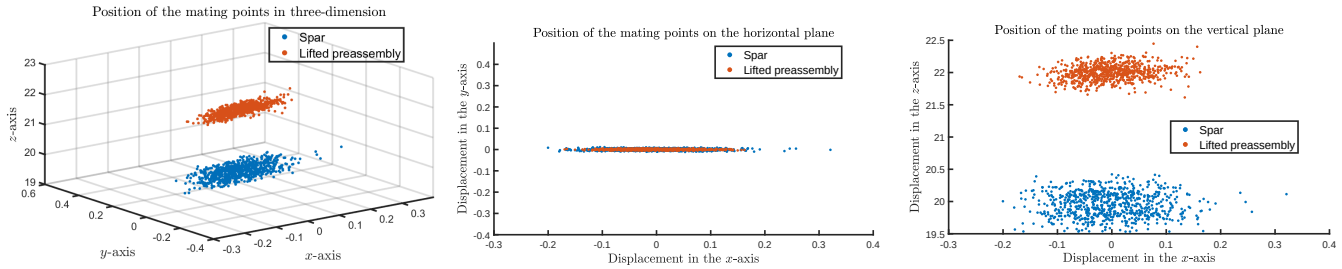

(a) The scatter of mating points in the three-dimension. **(b) The scatter of mating points on the horizontal plane.** **(c) The scatter of mating points on the vertical plane.**

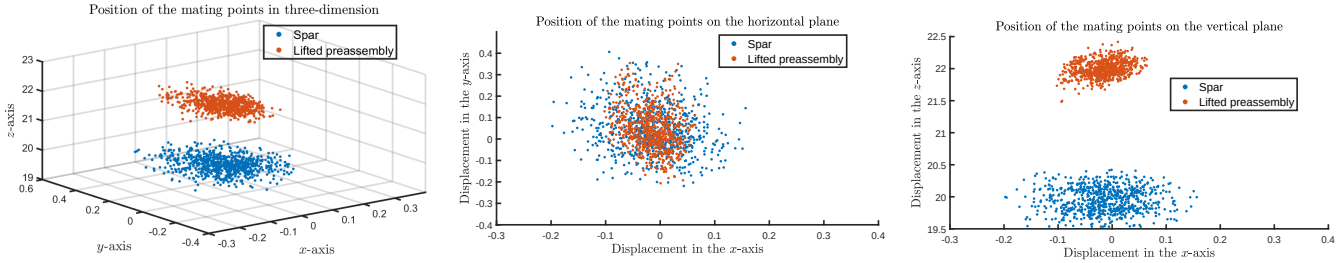

(d) The scatter of mating points in the three-dimension. **(e) The scatter of mating points on the horizontal plane.** **(f) The scatter of mating points on the vertical plane.**

FIGURE 6: The scatter of mating points in representative sea states for H_s=1 m, T_p=6 s, Seed=1 and varying wave directions, (a)-(c) denote wave direction = 0 deg, (d)-(f) denote wave direction = 120 deg.

4. SIMULATION RESULTS ANALYSIS AND NEURAL NETWORK PREDICTION MODEL

4.1 Simulation results

To investigate the relative motion of the mating points under different sea states, various sea states are selected to demonstrate the results. The scatter of mating points and the relative motions are shown in the horizontal, vertical, and three-dimensional planes. To make the images clearer, the scatter of mating points is plotted at every 25 sampling times.

Figure 6 and Figure 7 show the motions and relative motions of mating points in sea states with different wave directions. The other wave parameters (i.e., H_s = 1 m, T_p = 6 s, Seed=1) remain consistent. When the wave direction is 0 deg, the mating points move primarily along the x-axis. In contrast, when the wave is not in the direction of the vessel's length, the mating points produce a more extensive range of motions along the y-axis, mainly because the inertia moment of the vessel rotating around the y-axis is more significant. The maximum values of the relative motions also get larger on the horizontal plane. Fig.8 displays the relative motions of the mating points in selected sea state with H_s=1.9 m. The amplitude of the surge motions at the mating points increases, with a slight increase also observed in the amplitude of the heave motions. The maximum relative motions also get larger. Fig.9 displays the motions of the mating points in a sea state with larger T_p = 12 s. Increased motion range is observed at the mating points, particularly for the spar top point motion. The relative

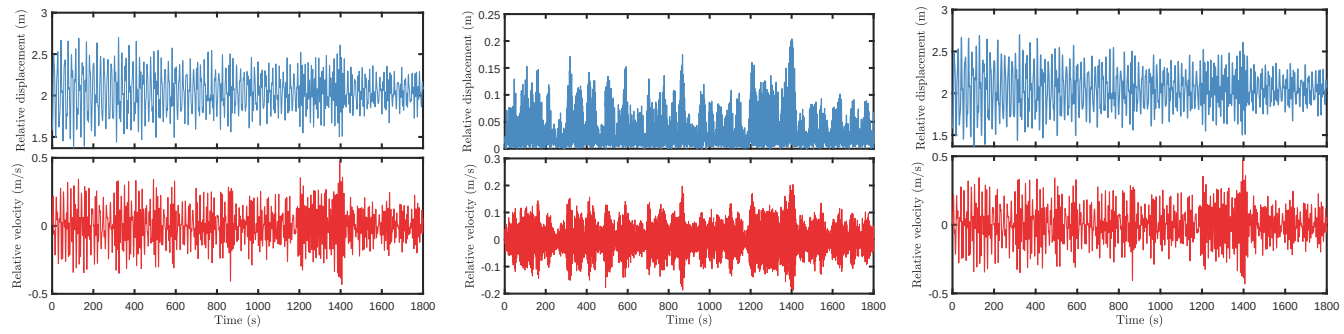

(a) Relative motions in the three-dimension.(b) Relative motions on the horizontal plane. (c) Relative motions on the vertical plane.

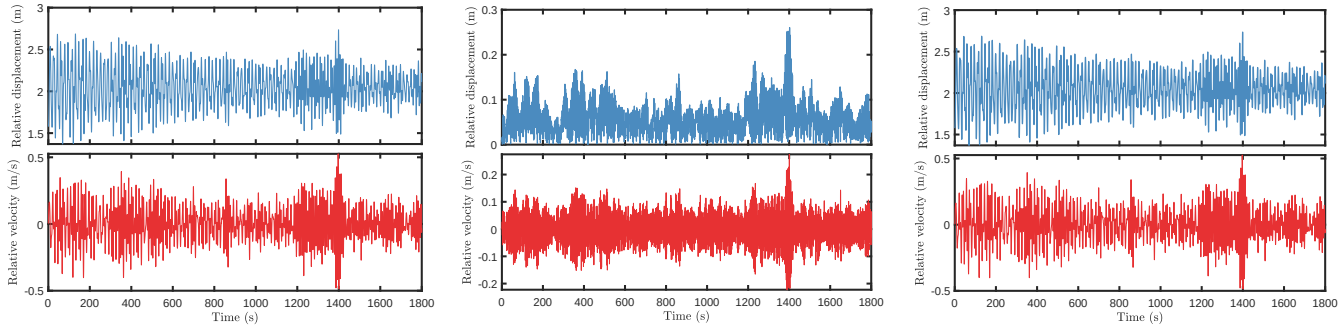

(d) Relative motions in the three-dimension.(e) Relative motions on the horizontal plane. (f) Relative motions on the vertical plane.

FIGURE 7: Relative motions of mating points for H_s=1 m, T_p=6 s, Seed=1, and direction=0 and relative motions of mating points in representative sea states for H_s=1 m, T_p=6 s, Seed=1 and varying wave directions, (d)-(f) denote wave direction = 0 deg,(g)-(i) denote wave direction = 120 deg.

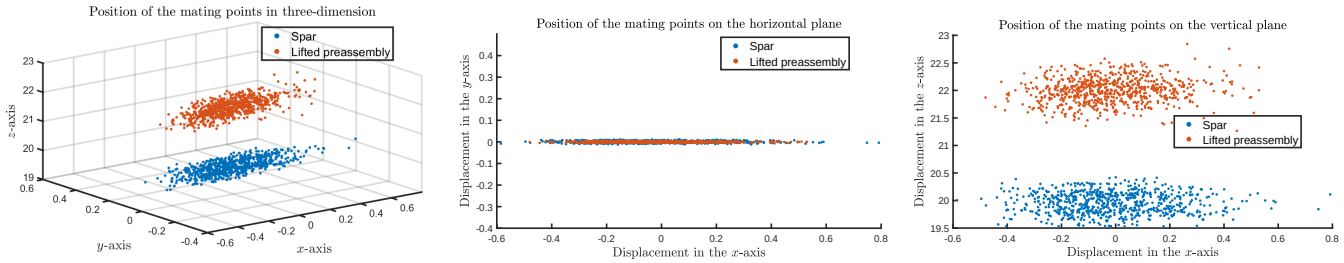

(a) The scatter of mating points in the three-dimension. (b) The scatter of mating points on the horizontal plane. (c) The scatter of mating points on the vertical plane.

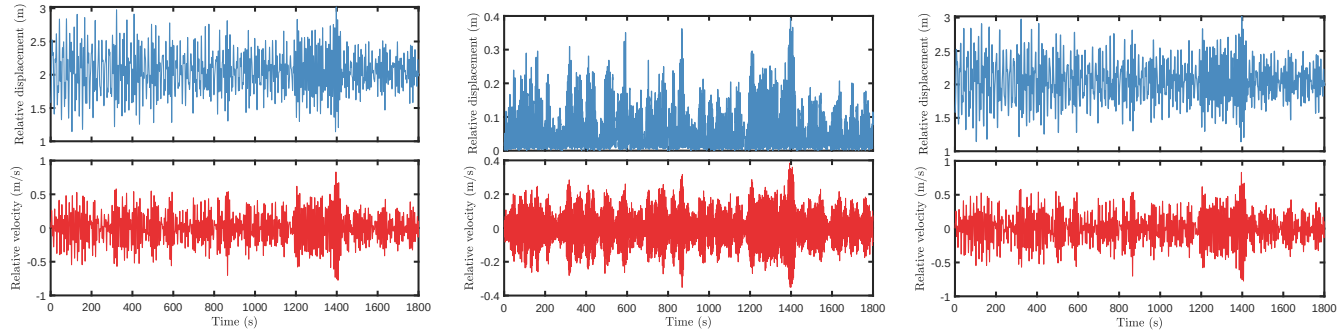

(d) Relative motions in the three-dimension.(e) Relative motions on the horizontal plane. (f) Relative motions on the vertical plane.

FIGURE 8: The scatter of mating points and relative motions of mating points in a representative sea state (H_s=1.9 m, T_p=6 s, Seed=1, Wave direction = 0 deg).

motions between the mating points are significantly magnified, resulting in a maximum relative displacement of up to about 4 m.

Figure 10 summarizes the detailed behavior of the maximum and minimum relative motions at sea states with various wave

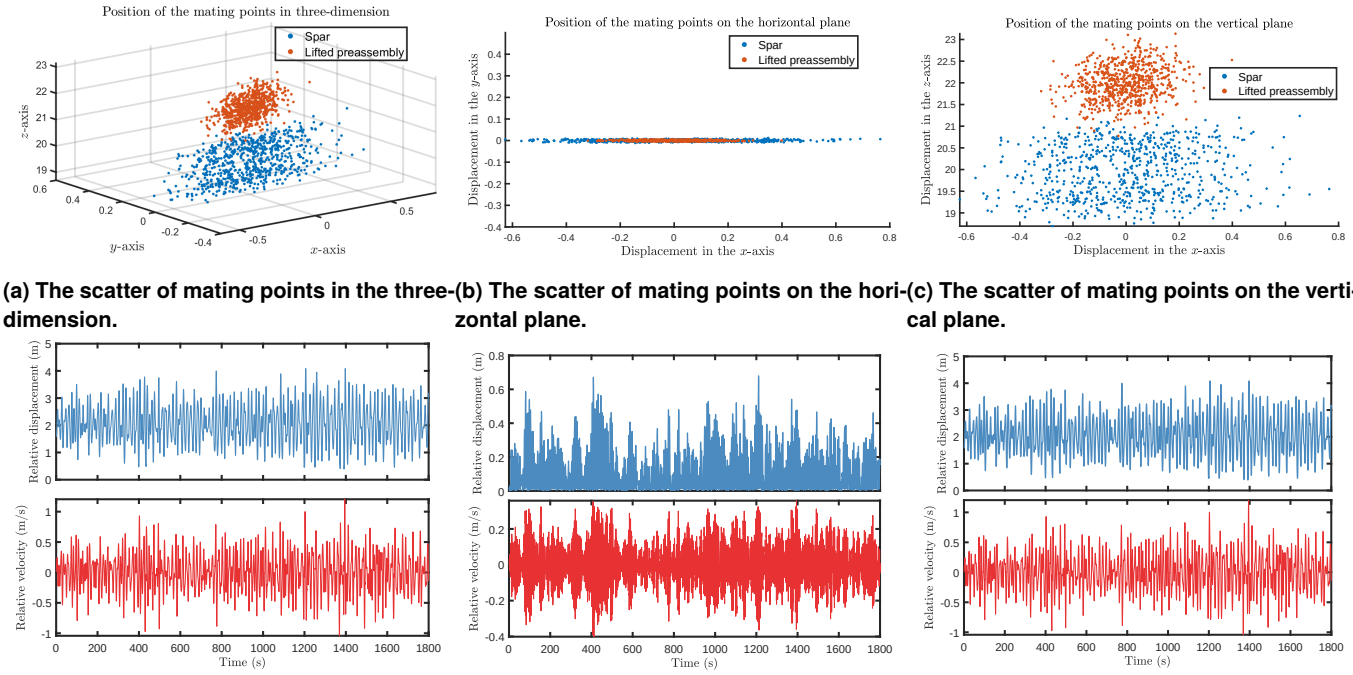

(a) The scatter of mating points in the three-dimension. **(b) The scatter of mating points on the horizontal plane.** **(c) The scatter of mating points on the vertical plane.**

(d) Relative motions in the three-dimension. **(e) Relative motions on the horizontal plane.** **(f) Relative motions on the vertical plane.**

FIGURE 9: The scatter of mating points and relative motions of mating points in a representative sea state (H_s=1 m, T_p=12 s, Seed=1, Wave direction = 0 deg).

parameters. It can be seen that the relative motions are more sensitive to H_s and T_p. Fig.10a presents an increase in the relative motion displacement between mating points as the T_p grows, showing a non-linear growth pattern. The maximum relative displacement reaches 4.08 m at T_p=12 s, which is 56.5% higher compared to the maximum relative displacement of 2.61 m at T_p = 6 s. In Fig.10c, increases in the maximum and minimum relative displacements and the magnitude of the minimum relative velocity are clearly observed as the H_s increases. The maximum relative displacement increases by an mean of 5% for every 0.3 m increment in H_s. The reason is mainly the correlation between the first-order motions and the wave height. Conversely, the maximum relative velocity shows the opposite trend. Positive and negative relative velocities reflect changes in different directions of the mating points. The increase in relative displacement causes the mating operation to get more complex and elevates the failure probability of the mating operation. Fig.10b and Fig.10d show that the relative motions are not sensitive to the wave direction and the wave seed set in Table 2.

4.2 Implement and results of the BP neural network

The 1260 high-fidelity simulations are obtained in Sima. Subject to the experimental conditions, the testing set also consists of simulations, and the data acting as the testing set does not participate in neural network training. The workflow of the prediction method is summarized in the following steps,

1. Obtain 1260 simulations, and split each simulation data using a 70%-30% time-based split.

2. The mean value of relative motion distance and the central moments of $2nd$ to $4th$ order, as well as the mean value of relative motion velocity and the central moments of $2nd$ to $4th$ order for the preceding 21 minutes (70% time series data of each simulation), are used as input variables. Calculate the maximum relative displacement, maximum relative velocity, minimum relative displacement, and minimum relative velocity of the final 9 minutes (representing 30% of the time series data of each simulation) to be set as the output values. Combine them into a complete dataset comprising 1260 cases, each with 8 inputs and 4 outputs. Both input values and output values are normalized.

3. The complete dataset is split into a training and testing set so that the training set is 1200 cases and the testing set is 60 cases.

4. The neural network model is trained using the training set.

5. The model is evaluated using the testing set. The accuracy indicators are used to evaluate the predicted effect of the established model. If the predicted effect is lower than expected, the hyperparameters are optimized and re-iterated starting from the third step.

After optimizing the hyper-parameters, (i.e., the number of hidden layers is set to 2, the number of neurons in each hidden layer is 15, and the learning rate is set to 0.01), the predicted model is constructed. The small amount of input variables and output variables results in a fast speed of constructing the model. The model can be constructed fast using the normalized values of the training set, i.e., only about 3 s to form the predicted model. Figure 11 demonstrates the results of the constructed BP neural network. The predicted effects of maximum relative displacement, maximum relative velocity, minimum relative displacement, and minimum relative velocity are shown, respectively. MSE are cal-

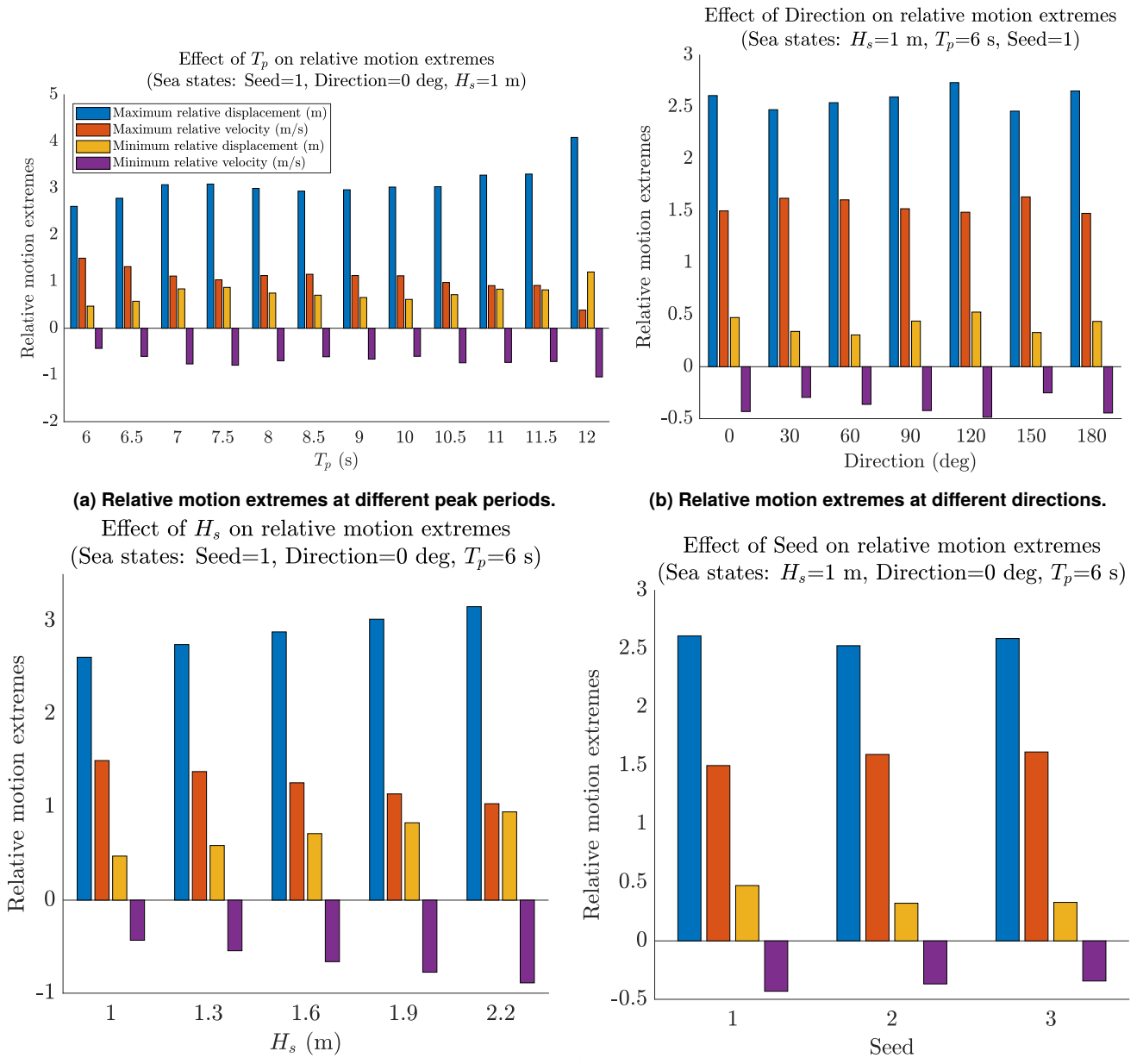

(a) Relative motion extremes at different peak periods.

(b) Relative motion extremes at different directions.

(c) Relative motion extremes at different significant wave heights.

(d) Relative motion extremes at different seed.

FIGURE 10: Relative motion extremes with different wave parameters

culated based on the maximum relative displacement, minimum relative displacement, maximum relative velocity, and minimum relative velocity, with values of 0.03, 0.008, 0.014, and 0.014, respectively. The prediction effect is excellent with the coefficient of determination R^2=0.95, 0.94, 0.90, and 0.92 calculated based on the maximum relative displacement, minimum relative displacement, maximum relative velocity, and minimum relative velocity, respectively. More data will further improve accuracy and robustness.

5. CONCLUSION

Previous studies for the conceptual tower-nacelle-rotor preassembly lifting method focused on the dynamic characteristics of structures, emphasizing the simulation of relative motion between the mating points. This research mainly introduces a method for predicting the relative motion between the mating points that can be used to assist practical engineering. In the initial work, relative motion is generated based on Sima. The effects of wave direction, spectral peak period, significant wave height, and wave seed on the relative motion are taken into account. Relative motions between mating points are more sensitive to changes in H_s and T_p. The prediction model constructed in this paper extracts the relative motion statistical characteristics as the input variables to predict the maximum and minimum values of relative motions. The results indicate that the model performs well in prediction, and the model has a fast computational speed. However, further complex marine environments and higher accuracy dynamics simulation are indispensable to verify the method.

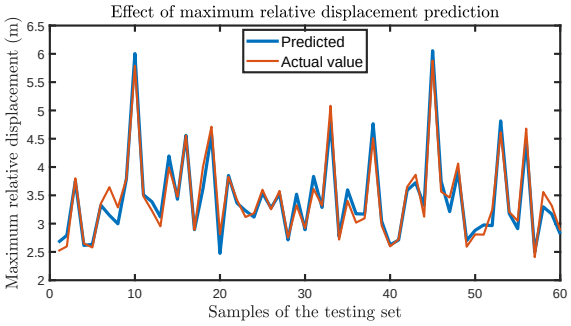

(a) Effect of maximum relative displacement prediction.

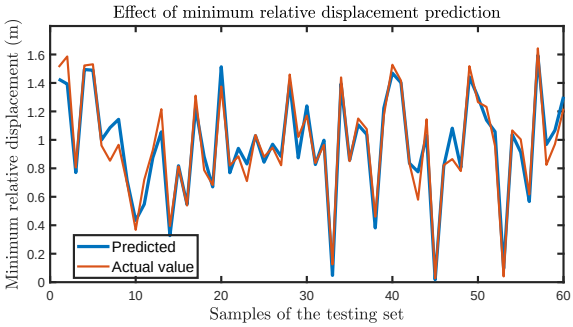

(b) Effect of minimum relative displacement prediction.

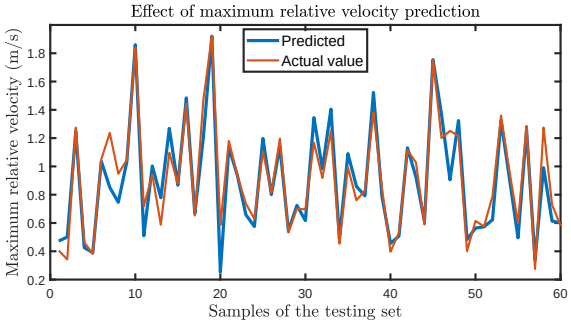

(c) Effect of maximum relative velocity prediction.

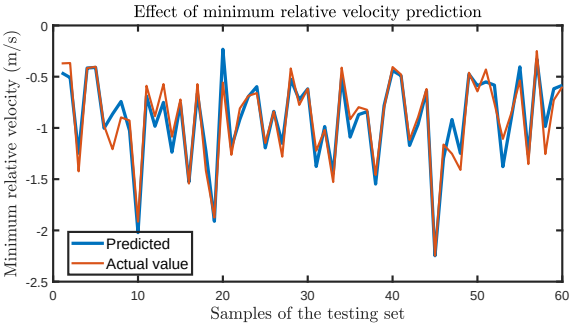

(d) Effect of minimum relative velocity prediction.

FIGURE 11: Prediction results of BP neural network.

REFERENCES

[1] Ringsberg, Jonas W., Daun, Viktor and Olsson, Fredrik. "Analysis of impact loads on a self-elevating unit during jacking operation." *Proceedings of the ASME 34th international conference on ocean, offshore and arctic engineering, 2015, Vol 3*. 2015. Amer Soc Mech Engn, Ocean Offshore & Arct Engn Div. 34th ASME International Conference on Ocean, Offshore and Arctic Engineering (OMAE2015), St John's, CANADA, MAY 31-JUN 05, 2015.

[2] Hatledal, Lars Ivar, Zhang, Houxiang, Halse, Karl Henning and Hildre, Hans Petter. "Numerical study for a catamaran gripper-monopile mechanism of a novel offshore wind turbine assembly installation procedure." *Proceedings of the ASME 36th international conference on ocean, offshore and arctic engineering , 2017, Vol 9*. 2017. ASME, Ocean Offshore & Arctic Engn Div. 36th ASME International Conference on Ocean, Offshore and Arctic Engineering, Trondheim, NORWAY, JUN 25-30, 2017.

[3] Jiang, Zhiyu, Li, Lin, Gao, Zhen, Halse, Karl Henning and Sandvik, Peter Christian. "Dynamic response analysis of a catamaran installation vessel during the positioning of a wind turbine assembly onto a spar foundation." *Marine Structures* Vol. 61 (2018): pp. 1–24. DOI 10.1016/j.marstruc.2018.04.010.

[4] Liu, Ting, Halse, Karl H., Leira, Bernt J., Jiang, Zhiyu, Chai, Wei, Brathaug, Hans-P. and Hildre, Hans P. "Dynamic response of a SWATH vessel for installing pre-assembled floating wind turbines." *Marine Structures* Vol. 88 (2023). DOI 10.1016/j.marstruc.2022.103341.

[5] Hassan, Mohamed and Guedes Soares, C. "Dynamic Analysis of a Novel Installation Method of Floating Spar Wind Turbines." *Journal of Marine Science and Engineering* Vol. 11 No. 7 (2023). DOI 10.3390/jmse11071373. URL https://www.mdpi.com/2077-1312/11/7/1373.

[6] Ren, Zhengru, Skjetne, Roger, Verma, Amrit Shankar, Jiang, Zhiyu, Gao, Zhen and Halse, Karl Henning. "Active heave compensation of floating wind turbine installation using a catamaran construction vessel." *Marine Structures* Vol. 75 (2021). DOI 10.1016/j.marstruc.2020.102868.

[7] Hong, Sunghun, Zhang, Houxiang, Nord, Torodd Skjerve and Halse, Karl Henning. "Effect of fender system on the dynamic response of onsite installation of floating offshore wind turbines." *Ocean Engineering* Vol. 259 (2022). DOI 10.1016/j.oceaneng.2022.111830.

[8] Ataei, Behfar, Yuan, Shuai, Ren, Zhengru and Halse, Karl Henning. "Effects of structural flexibility on the dynamic responses of low-height lifting mechanism for offshore wind turbine installation." *Marine Structures* Vol. 89 (2023): p. 103399. DOI https://doi.org/10.1016/j.marstruc.2023.103399. URL https://www.sciencedirect.com/science/article/pii/S0951833923000321.

[9] Kaplan, Paul. "A Study of Prediction Techniques for Aircraft Carrier Motions at Sea." *Journal of Hydronautics* Vol. 3 No. 3 (1969): p. 121–131. DOI 10.2514/3.62814.

[10] Triantafyllou, M., Bodson, M. and Athans, M. "Real time estimation of ship motions using Kalman filtering tech-

niques." *IEEE Journal of Oceanic Engineering* Vol. 8 No. 1 (1983): pp. 9–20. DOI 10.1109/JOE.1983.1145542.

[11] Chung, JC, Bien, Z and Kim, YS. "A note on ship-motion prediction based on wave-excitation input estimation." *IEEE Journal of Oceanic Engineering* Vol. 15 No. 3 (1990): pp. 244–250. DOI 10.1109/48.107153.

[12] Nielsen, Ulrik D., Brodtkorb, Astrid H. and Jensen, Jorgen J. "Response predictions using the observed autocorrelation function." *Marine Structures* Vol. 58 (2018): pp. 31–52. DOI 10.1016/j.marstruc.2017.10.012.

[13] Jiang, Hua, Duan, ShiLiang, Huang, Limin, Han, Yang, Yang, Heng and Ma, Qingwei. "Scale effects in AR model real-time ship motion prediction." *Ocean Engineering* Vol. 203 (2020). DOI 10.1016/j.oceaneng.2020.107202.

[14] Takami, Tomoki, Nielsen, Ulrik Dam and Jensen, Jorgen Juncher. "Real-time deterministic prediction of wave-induced ship responses based on short-time measurements." *Ocean Engineering* Vol. 221 (2021). DOI 10.1016/j.oceaneng.2020.108503.

[15] Schirmann, Matthew L., Collette, Matthew D. and Gose, James W. "Data-driven models for vessel motion prediction and the benefits of physics-based information." *Applied Ocean Research* Vol. 120 (2022). DOI 10.1016/j.apor.2021.102916.

[16] Khan, Ameer A., Marion, Kaye E., Bil, Cees and Simic, Milan. "Motion Prediction for Ship-Based Autonomous Air Vehicle Operations." DePietro, G, Gallo, L, Howlett, RJ and Jain, LC (eds.). *Intelligent Interactive Multimedia Systems And Services 2016*, Vol. 55: pp. 323–333. 2016. KES Int. DOI 10.1007/978-3-319-39345-2_28. 9th KES International Conference on Intelligent Interactive Multimedia Systems and Services (IIMSS), Puerto de la Cruz, SPAIN, JUN 15-17, 2016.

[17] Huang, Bai-Gang, Zou, Zao-Jian and Ding, Wei-Wei. "Online prediction of ship roll motion based on a coarse and fine tuning fixed grid wavelet network." *Ocean Engineering* Vol. 160 (2018): pp. 425–437. DOI 10.1016/j.oceaneng.2018.04.065.

[18] Yin, Jian-Chuan, Zou, Zao-Jian, Xu, Feng and Wang, Ni-Ni. "Online ship roll motion prediction based on grey sequential extreme learning machine." *Neurocomputing* Vol. 129 No. SI (2014): pp. 168–174. DOI 10.1016/j.neucom.2013.09.043.

[19] Li, Song, Wu, Wenhua and Yao, Weian. "Bayesian based updating of hull and mooring structure parameters of semi-submersible platforms using monitoring data." *Ocean Engineering* Vol. 272 (2023). DOI 10.1016/j.oceaneng.2023.113865.